# Epitaxial Growth of RuO 2 (100) on Ru(10$\bar{1}$0): Surface Structure and Other Properties

**ARTICLE** *in* THE JOURNAL OF PHYSICAL CHEMISTRY B · MARCH 2001

Impact Factor: 3.3 · DOI: 10.1021/jp003650y

# Epitaxial Growth of $RuO_2(100)$ on $Ru(10\bar{1}0)$: Surface Structure and Other Properties

**Y. D. Kim, S. Schwegmann, A. P. Seitsonen,† and H. Over***

*Department of Physical Chemistry, Fritz-Haber-Institut der Max-Planck-Gesellschaft, Faradayweg 4-6, D-14195 Berlin, Germany*

*Received: October 5, 2000; In Final Form: January 4, 2001*

We determined the surface structure of $RuO_2(100)$ formed on $Ru(10\bar{1}0)$ by employing the techniques of low-energy electron diffraction (LEED) and density functional theory (DFT) calculations. The $RuO_2(100)$ film grows lattice-matched with its [010] direction along the [0001] direction of $Ru(10\bar{1}0)$ (4.5% compressively strained), while it grows incommensurately with the [001] direction of $RuO_2(100)$ along the $[\bar{1}2\bar{1}0]$ direction of $Ru(10\bar{1}0)$. The $RuO_2(100)$ surface is terminated by bridging O atoms, which are attached to the coordinatively unsaturated Ru (cus-Ru) atoms with a bond length of 2.01 Å. The other Ru−O bond lengths are in the range of 1.90−2.05 Å, typical for bulk $RuO_2$. Due to the presence of cus-Ru atoms on $RuO_2(100)$, CO molecules adsorb quite strongly as evidenced by a desorption state at 300−400 K. The activity of the $RuO_2(100)$ surface for the CO oxidation reaction is similar to that of $RuO_2(110)$. The surface energies of $RuO_2(110)$ and $RuO_2(100)$ are 71 and 87 meV/Å$^2$, respectively.

## 1. Introduction

The oxygen-rich Ru(0001) surfaces with more than 3 monolayers of oxygen are extraordinarily active in the oxidation of CO molecules, while the corresponding metallic phase is virtually inactive.[1−3] Only recently, the surface structure of this active phase was determined by a combined low-energy electron diffraction/density functional theory (LEED/DFT) analysis.[4,5] Oxygen-rich Ru(0001) surfaces beyond a coverage of 3 monlayers of oxygen consist of areas of (1 × 1)-O overlayers in coexistence with patches of ruthenium dioxide $RuO_2$ in (110) orientation. Both domains extend over several 10 $\mu$m across the surface as imaged by scanning tunneling microscopy (STM).[4,6] The catalytically active part of the O-rich phase on Ru(0001) was found to be $RuO_2(110)$, and the active centers on the oxide were identified with the coordinatively unsaturated Ru sites (cus-Ru).[4] The $RuO_2(110)$ domains grow epitaxially on Ru(0001) and are aligned with its $[\bar{1}10]$ axis along the three $[10\bar{1}0]$ high-symmetry directions of the Ru(0001) substrate producing a 3-fold mosaic microstructure. From the LEED pattern the dimensions of the real space unit cell were estimated to be (6.4 ± 0.3 Å × 3.1 ± 0.2 Å), which agrees favorably with the unit cell of a $RuO_2(110)$-(1 × 1) surface, i.e., 6.38 Å × 3.11 Å. These lattice parameters are not simply related to the centered unit cell (4.69 Å × 2.71 Å) of the Ru(0001) surface (cf. Figure 1). As a consequence of the small corrugation of Ru(0001), the $RuO_2(110)$ domains grow incommensurately to the underlying Ru(0001) substrate. The incommensurability of the $RuO_2(110)$ film on Ru(0001) suggests the presence of unstrained oxide domains.

Oxygen-rich phases on Ru(0001) can also be synthesized via an electrochemical route, again exposing (1 × 1)-O and $RuO_2$ domains.[7] The $RuO_2$ areas were however quite rough and, somewhat to our surprise, oriented with the (100) face parallel to the Ru(0001) surface. The $RuO_2(100)$ domains also grow epitaxially and incommensurately. The latter effect suggests again that the oxide film is unstrained. Together with the gas-phase growth of $RuO_2(110)$ on Ru(0001), one may therefore infer that the surface energies of both faces of $RuO_2$ are almost degenerated so that its actual orientation may essentially be governed by kinetics.

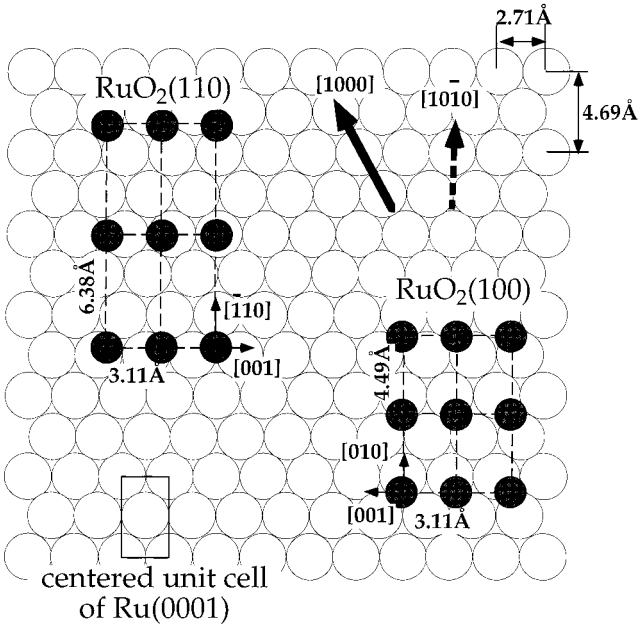


**Figure 1.** Schematic (top view) of the domains of $RuO_2(110)$ and $RuO_2(100)$ on Ru(0001) which are aligned along the [1000] and $[10\bar{1}0]$ directions of the Ru(0001) substrate. Important dimensions and directions are indicated.

The bulk-truncated $RuO_2(100)$ surface has a rectangular unit cell of dimensions 4.49 and 3.11 Å. The long side matches the periodicity of the Ru(0001) in the $[10\bar{1}0]$ direction (4.69 Å) within 4.5%; the $RuO_2(100)$ would be expanded along the [010]

† Also at: INFM, Unità di Roma, Dipto. di Fisica, Università La Sapienza, P.'le A. Moro 2, I-00185 Rome, Italy, and IPP Garching, Boltzmannstr. 2, D-85748 Garching, Germany.

* To whom correspondence should be addressed. Fax: ++49−30−84135106. E-mail: over@fhi-berlin.mpg.de (URL: http://w3.rz-berlin.mpg.de/pc/).

10.1021/jp003650y CCC: $20.00 
Published on Web 02/24/2001

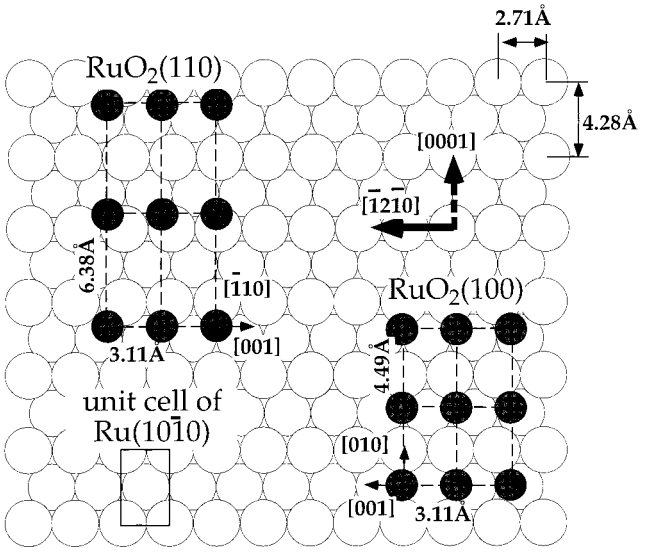


**Figure 2.** Schematic (top view) of the domains of $RuO_2(110)$ and $RuO_2(100)$ on $Ru(10\bar{1}0)$ which are aligned along the [0001] and $[12\bar{1}0]$ directions of the $Ru(10\bar{1}0)$ substrate. Important dimensions and directions are indicated. The light shadowed substrate atoms are lying deeper by 0.8 Å.

direction (cf. Figure 1) in order to match the Ru(0001) lattice along the [0001] direction. As $RuO_2(100)$ grows incommensurately on the Ru(0001) surface, the corrugation of the potential energy surface of the Ru(0001) substrate is obviously not sufficiently high to enforce commensurability along the $[10\bar{1}0]$ direction.

In going to a more corrugated potential energy surface such as that provided by the $Ru(10\bar{1}0)$ surface, one may anticipate that now the propensity to form a $RuO_2(100)$ film, which is at least lattice-matched along one high-symmetry direction of the substrate, may be higher and therefore allows for the growth of $RuO_2(100)$ even under ultrahigh-vacuum conditions. Recall that the unit cell dimensions of Ru(100) are 4.28 Å × 2.71 Å; i.e., the lattice mismatch between $Ru(10\bar{1}0)$ and $RuO_2(100)$ along the long axis is only 4.5% (cf. Figure 2). The lattice mismatch between $RuO_2(110)$ and $Ru(10\bar{1}0)$ is much larger (6.38 Å × 3.11 Å) (cf. Figure 2) so that $RuO_2(110)$ should not grow on $Ru(10\bar{1}0)$ if the interfacial energy is dominating the energy balance. For lattice matching along the [0001] direction the $RuO_2(100)$ surface has to be contracted along the [010] direction, which of course costs deformation energy in comparison with a fully relaxed $RuO_2(100)$ film but leads to an energy gain due to the more favorable interfacial energy.

In fact, we show in this contribution that the oxidation of the $Ru(10\bar{1}0)$ surface leads to the growth of a $RuO_2(100)$ film, which is pseudomorph along the [0001] direction of $Ru(10\bar{1}0)$. As the $RuO_2(100)$ is compressed along the [010] direction, the vertical atomic positions differ from corresponding bulk positions of $RuO_2(100)$.

## 2. Experimental and Theoretical Details

The measurements were conducted in an ultrahigh-vacuum chamber that is equipped with a four-grid back-view LEED optics, Auger electron spectroscopy (AES), thermal desorption spectroscopy (TDS), and facilities to clean and prepare the $Ru(10\bar{1}0)$ surface.[8] The sample temperature could be varied from 100 K (by cooling with liquid $N_2$) to 1530 K (by direct resistive heating). The LEED intensities as a function of the incident energy of the electrons were collected at normal incidence of the primary beam, while keeping the sample temperature at 100 K. A computer-controlled high-sensitive CCD camera system was used to record spot intensities from the LEED fluorescence screen. LEED *I*/*E* curves were computed by using the program code of Moritz[9] and compared with the experimental LEED *I*/*E* curves by applying a least-squares optimization algorithm,[10] based on Pendry's *r*-factor $R_P$.[11]

For the DFT calculations we employed the generalized gradient approximation of Perdew et al.[12] for the exchange-correlation functional and used ab initio pseudopotentials in the fully separable form.[13] The surface was modeled by five double layers of $RuO_2(100)$ (supercell approach). Consecutive $RuO_2(100)$ slabs were separated by a vacuum region of about 16 Å. Calculations were performed using a (1 × 1) surface unit cell. For the autocompensated surfaces of $RuO_2$ (such as the bridging oxygen terminated (100) and the (110) faces) the surface energy $\gamma$ is simply given by

$$\gamma A = (1/2)[E_{\mathrm{slab}} - \mu(\mathrm{RuO_2})N_{\mathrm{Ru}}] \qquad (1)$$

with the area of the unit cells $A = 14.25$ Å$^2$ ((100) face) and $A = 21.28$ Å$^2$ ((110) face). $\mu(RuO_2)$ is the energy of bulk $RuO_2$ per $RuO_2$ unit, $N_{Ru}$ is the number of $RuO_2$ units in the supercell of the $RuO_2$ slab, and $E_{slab}$ is the total energy of the $RuO_2$ slab. The prefactor 1/2 accounts for the presence of two surfaces of the $RuO_2$ slab.

The $Ru(10\bar{1}0)$ sample was cleaned by argon ion bombardment at 1 keV followed by cycles of oxygen adsorption and thermal desorption in order to remove surface carbon. Final traces of oxygen were removed by flashing the surface to 1530 K, resulting in a sharp (1 × 1) LEED pattern and the absence of impurity losses in AES. This procedure was successfully applied in a recent study of the surface structures of O overlayers on $Ru(10\bar{1}0)$.[14]

The oxide phases were produced by exposing a well-prepared single-crystal $Ru(10\bar{1}0)$ to high doses of $O_2$ or $NO_2$ at elevated sample temperatures of 600−770 K. $NO_2$ was dosed by backfilling the ultrahigh-vacuum chamber. To reduce the $O_2$ background pressure in the ultrahigh-vacuum chamber during exposure, oxygen was dosed through a glass capillary array doser (with channels 3 mm long and 10 $\mu$m wide, total transparency of 50%) about 1 mm away from the sample. In this way, the local $O_2$ pressure at the sample could be enhanced by a factor of about 100. Typical oxygen exposures for the oxide preparation were about "6000" langmuirs (determined by the ion gauge reading times exposure time: corresponding doses are given in quotation marks); recall that the actual exposure is about 100 times higher. For the case of Ru(0001) "60 000" langmuirs at 800 K were required to produce the same oxygen load as on $Ru(10\bar{1}0)$, leading to the epitaxial growth of a $RuO_2(110)$ film. This finding is consistent with the intuitive notion that open surfaces are more prone to oxidation. After the background pressure in the ultrahigh-vacuum chamber has reached a value below $10^{-9}$ mbar, the sample was briefly annealed to 600 K to remove contamination by residual gas adsorption. Subsequently, the sample was cooled to the measuring temperature of 100 K.

Identical oxide structures on $Ru(10\bar{1}0)$ were produced by $NO_2$ exposure, a very efficient oxidant and source of atomic oxygen; we already applied $NO_2$ exposure successfully to produce the (1 × 1)-O and the (2 × 2)-3O overlayer phases on Ru(0001).[15,16] The oxidation of $Ru(10\bar{1}0)$ by $NO_2$ is, however, different from the Ru(0001) case for which only excessive $NO_2$ exposures lead to an oxidation of the sample. Beyond the (1 × 1)-O overlayer, the atomic oxygen supplied by $NO_2$ exposure is first dissolved in the near-surface region of Ru(0001) without forming an

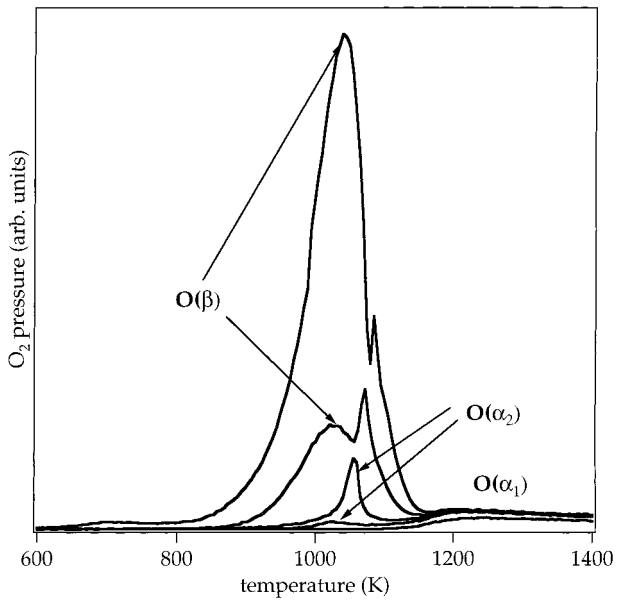


**Figure 3.** Thermal oxygen desorption spectrum of the $Ru(10\bar{1}0)$-(2 × 1)-p2mg-2O (O(α) having the lowest coverage among the TD traces). $O_2$ TD spectra are also shown for the high O coverage phases on Ru-$(10\bar{1}0)$, prepared by $NO_2$ exposure of 60, 80, 290, and 2000 langmuirs, respectively (heating rate, 5 K/s; $T = 600$ K). The chemisorbed oxygen is denoted by $O(\alpha_1)$; the oxidic oxygen species, by $O(\beta)$. $O(\alpha_2)$ is assigned to a precursor state for oxidic oxygen on Ru.

oxide.[3] LEED always displayed a (1 × 1) pattern, and the analysis of the LEED *I*/*E* curves proved the presence of a perfect (1 × 1)-O overlayer on Ru(0001) and no (i.e., "invisible" for LEED) oxygen in the near-surface region.

### 3. Results and Discussion

**3.1. Thermal Stability of $RuO_2(100)$.** Recently, we analyzed the c(2 × 4)-2O and the (2 × 1)-p2mg-2O overlayer structures on the $Ru(10\bar{1}0)$ surface at O coverages of 0.5 and 1.0, respectively, by LEED and DFT.[14] The thermal desorption spectrum (TDS) and the LEED pattern of the (2 × 1)-p2mg-2O overlayer are depicted in Figures 3 and 4a, respectively. The desorption state of chemisorbed atomic oxygen on $Ru(10\bar{1}0)$ is denoted by $O(\alpha_1)$. In Figure 3 we also superimpose the oxygen TD spectra of the high-density O phases, which were prepared by $NO_2$ exposure. As a function of the $NO_2$ exposure, first a desorption state at 1030 K emerges which shifts toward higher temperatures with increasing coverage. The presence of this new desorption state $O(\alpha_2)$ is accompanied by the development of a streaky (1 × 2) LEED pattern (cf. Figure 4b); initially it coexists with the (2 × 1)-p2mg-2O, but at a coverage of about 2 monolayers (estimated by AES) only a streaky (1 × 2) LEED pattern remains. A streaky (1 × 2) LEED pattern tells us that the periodicity of the superstructure is mostly 2 but sometimes also 3, 4, 5, and so on. Further exposure of $NO_2$ leads to an additional desorption state at 1025 K ($O(\beta)$) and the appearance of a (0.86 × 1) LEED pattern (cf. Figure 4c,d). Again in the intermediate coverage region the (1 × 2) coexists with the (0.86 × 1) structure (cf. Figure 4c), but eventually all spots with (1 × 2) and also with (1 × 1) periodicity diminished (cf. Figure 4d). The O coverage at the final stage was estimated by AES to be about 20 monolayers. Apparently, the entire $Ru(10\bar{1}0)$ surface is covered by an oxide film. In real space the (0.86 × 1) LEED pattern transforms to a rectangular unit cell with dimensions 4.28 Å × 3.11 Å; note that due to the commensurability of the long axis with the substrate, the value of 4.28 Å is precisely known, while that of 3.11 Å is uncertain within 4−5%.

Previously, similar TD spectra as a function of oxygen exposure were reported by Klein et al.[17] It should, however, be mentioned that neither a "supercompressed" (4 × 2)-p2gg oxygen structure[18] nor a c(2 × 6) structure[19] could be identified in our study. Assuming that the saturation structure is a compressed $RuO_2(100)$ surface structure (which will be proven by the present LEED/DFT analysis discussed below), the (1 × 2) structure may be regarded as the initial stage for oxide formation, which may offer the challenging prospect of studying the actual oxidation process of the $Ru(10\bar{1}0)$ surface in more detail. An identical sequence of O surface structures was observed upon extensive $O_2$ exposure of the $Ru(10\bar{1}0)$ surface at 600 K. In Figure 5 corresponding TD spectra are summarized, which are identical to those prepared by $NO_2$ exposure (cf. Figure 3). The oxygen desorption spectrum alters, however, even qualitatively if the oxygen exposure is carried out at a sample temperature of 770 K. Figure 6b shows a typical $O_2$ TD spectrum for $O_2$ exposure at 770 K in comparison with those prepared at 600 and 660 K. First, with higher sample temperature, more oxygen is incorporated in the near-surface region. A similar behavior was encountered with the system O−Ru-(0001).[3] For the preparation at 600 and 660 K the desorption temperature of the main $O_2$ peak is at 1040 K, while for a preparation temperature of 770 K a single desorption state at 1100 K emerges. The LEED pattern of this high-temperature phase exhibits c(2 × 2) symmetry with respect to the compressed $RuO_2(100)$ surface. The TD spectra suggest that the $RuO_2(100)$-c(2 × 2) is more stable than the $RuO_2(100)$-(1 × 1).

DFT calculations determined the (1 × 1) surface energies of the (110) and the (100) faces of $RuO_2$ to be 71 and 87 meV/Å$^2$, respectively (cf. Figure 7). To produce the (110) or the (100) surface of $RuO_2$ by cleavage, two Ru−O bonds per unit cell have to be broken; i.e., on $RuO_2(100)$ the averaged energy to break a bond is 1.21 eV, while on $RuO_2(110)$ this value is 1.41 eV. Obviously, the direct coordination of cus-Ru and bridging oxygen atoms on $RuO_2(100)$ allows for a better relaxation than on $RuO_2(110)$ where cus-Ru and bridging O atom are well-separated (cf. Figure 7). The higher surface energy of $RuO_2$-(100) is just a consequence of the higher density of undercoordinated O and Ru atoms at the (100) surface. From a surface energy point of view the (110) face is clearly preferred. However, it is interesting to note that the $RuO_2(100)$-c(2 × 2) surface is thermally even more stable than the $RuO_2(110)$ film on Ru(0001) (cf. Figure 6a), suggesting an even lower surface energy of $RuO_2(100)$-c(2 × 2) in comparison with $RuO_2(110)$−(1 × 1).

Actually, the (1 × 1) and the c(2 × 2) surface structures coexist on $RuO_2(100)$ for preparation temperatures, ranging from 700 to 800 K. This was concluded from CO adsorption experiments, which indicate that only the (1 × 1) LEED spots are affected by CO exposure at room temperature, but not the genuine c(2 × 2) spots (neither the absolute intensity nor the structure of the LEED *I*/*E* curves). Since the $RuO_2(100)$-c(2 × 2) is thermally more stable than the corresponding (1 × 1) surface, we surmise the c(2 × 2) surface to be a reconstructed $RuO_2(100)$ surface.

**3.2. Surface Structure of $RuO_2(100)$.** In the LEED analysis of $RuO_2(100)$-(1 × 1) we tested two essentially different structure models in a wide range of parameter space, namely, the bulk-truncated $RuO_2(100)$ surfaces either terminated with Ru atoms or terminated with rows of bridging oxygen atoms;

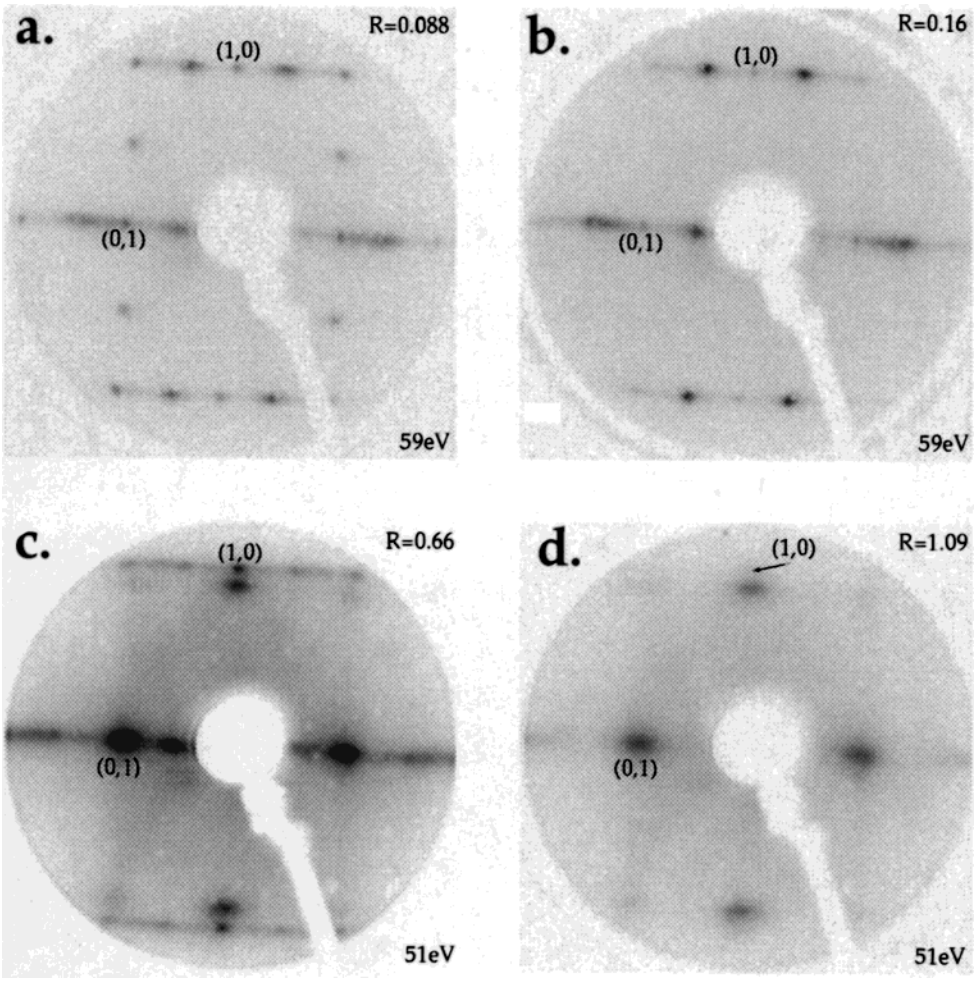


**Figure 4.** LEED pattern of the oxygen-rich phases of Ru(10$\bar{1}$0): (a) (2 × 1)-p2mg-2O; (b) (1 × 2) with 2 monolayers of oxygen; (c) (0.86 × 1) in coexistence with the (1 × 2): 8 monolayers of oxygen; (d) (0.86 × 1) with 20 monolayers of oxygen. The oxygen coverages are estimated by the ratio of the AES peak heights of O and Ru given by *R*.

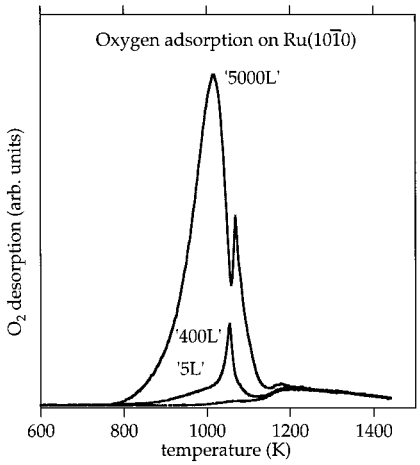


**Figure 5.** Thermal oxygen desorption spectra of O-rich phases on Ru-(10$\bar{1}$0) prepared by excessive $O_2$ exposures at 600 K sample temperature, using the microcapillary array doser (exposures are given in "langmuirs"; heating rate, 3 K/s).

the lateral lattice constant was adopted from the LEED pattern to be 4.28 Å × 3.11 Å. Our LEED analysis entered an experimental data set of seven beams covering a cumulative energy range of 1340 eV taken at 100 K and normal incidence of the electron beam. From the LEED analysis a clear preference was given to the termination with bridging oxygen atoms. The best *r*-factors achieved with these models were 0.32 and 0.41 for the O- and the Ru-terminated $RuO_2$(100) surface, respectively. The oxygen-terminated $RuO_2$(110) surface can be considered as a nonpolar microscopically rough surface.

The optimum surface structure as determined by the LEED analysis is summarized in Figure 8. The oxide surface is terminated by bridging oxygen atoms and is therefore fully compatible with a stoichiometric $RuO_2$(100) surface. The termination by bridging oxygen atoms is reasonable since it leads to an autocompensated (charge neutral) surface; i.e., the reduction in coordination number is the same for oxygen and ruthenium atoms on the surface, while the Ru-terminated surface is not autocompensated. The LEED intensity spectra for the best-fit geometry of the $RuO_2$(110) surface are reproduced in Figure 9.The structure of bulk $RuO_2$(100) is characterized by bare Ru layers, which are separated by buckled (0.45 Å) O bilayers. The Ru−O layer distance is 0.90 Å. The main structural characteristic of the compressed $RuO_2$(100) surface structure is that the top O bilayer is strongly puckered (with a buckling amplitude of 0.69 Å instead of 0.45 Å), maintaining the layer distance between the first and second Ru plane of 2.26 Å. The Ru−O bond length between the bridging O and the coordinated Ru atom is 2.01 Å, which is identical to the bulk value. The other Ru−O bond lengths have reasonable values between 1.90 and 2.05 Å. The driving force for the observed relaxations of $RuO_2$-(100) may be seen either as a response to the unidirectional compression of the $RuO_2$(100) surface or it may be considered as an inherent structural element of the $RuO_2$(100) surface. DFT

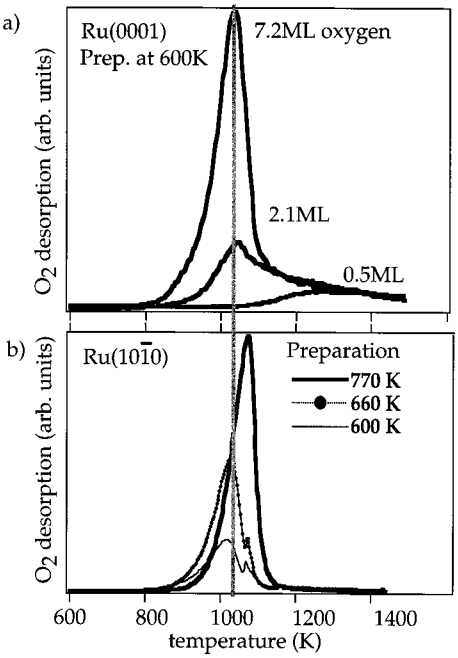


**Figure 6.** (a) For comparison, thermal desorption spectra of O-rich phases on Ru(0001) (heating rate, 3 K/s) for various oxygen coverages. The oxygen-rich phases are produced by exposing large amounts of oxygen to a Ru(0001) surface kept at 600 K. (b) Thermal oxygen desorption spectra of O-rich phases on Ru(10$\bar{1}$0). The $O_2$ exposure was in all cases "6000" langmuirs with the glass capillary doser. With sample temperatures of 600 and 660 K during $O_2$ exposure a (0.86 × 1) surface structure was prepared. The temperature of the desorption states are identical for both preparation temperatures and compares well with that found for O-rich phases on Ru(0001). At a preparation temperature of 770 K much more oxygen is accommodated in the surface region, and the temperature of the main desorption state is shifted by 30 K. LEED indicates a c(2 × 2) superstructure with respect to the (0.86 × 1) unit cell (heating rate, 3 K/s).

calculations of a relaxed and an unidirectional strained oxide film disclosed that the experimentally observed strong buckling is solely due to strain effects. The optimized structural parameters obtained by DFT calculations for the strained $RuO_2(100)$ film are included in Figure 8 (values in parentheses). The agreement between DFT and LEED is excellent with respect to the vertical parameters. Similar to the $RuO_2(110)$ surface, the surface of the $RuO_2(100)$ film on Ru(10$\bar{1}$0) exposes cus-Ru atoms and undercoordinated (i.e. bridging) O atoms. However, these undercoordinated Ru and O atoms are attached to each other on $RuO_2(100)$, in contrast to $RuO_2(110)$, where these undercoordinated Ru and O atoms are well-separated. This may have profound consequences for the catalytic activity and selectivity of these surfaces for the partial oxidation of hydrocarbons, for instance.

It is interesting to note that a compression of 4.5% along the [100] direction alters only marginally the Ru−O bond length in the bulk-truncated $RuO_2(100)$ surface. This is quite different from the $RuO_2(110)$ surface. To compress the unit cell of $RuO_2$-(110) along the [001] and [$\bar{1}$10] directions, the Ru−O bond lengths change more drastically and therefore cost more energy. This behavior is also reflected by the large anisotropy of 2.6 in the linear compressibilities of $RuO_2$; i.e., the linear compressibility along the [010] direction is by a factor of 2.6 larger, and therefore softer, than along the [001] direction.[20,21]

**3.3. Chemical Activity.** The presence of cus-Ru atoms on the $RuO_2(100)$ surface is also supported by the CO adsorption/desorption experiments. CO molecules adsorb quite strongly on the $RuO_2(100)$ surface with a binding energy of 0.7 eV (DFT

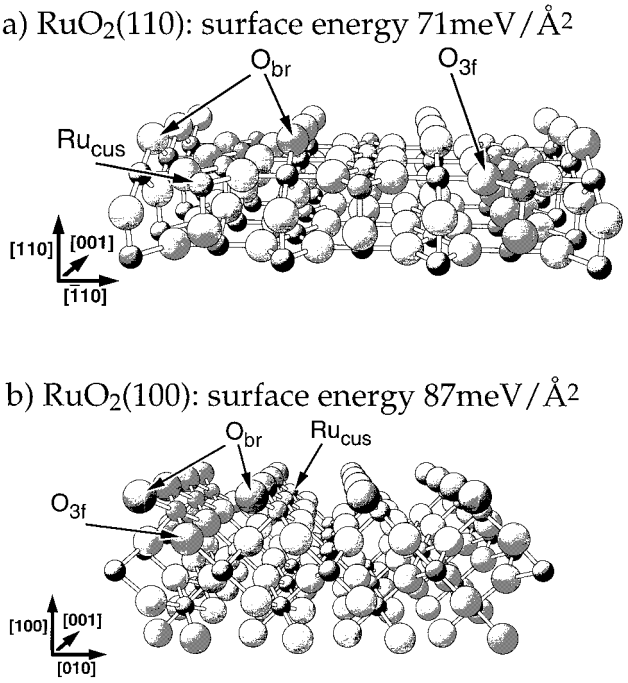


**Figure 7.** Ball-and-stick model of the bridging oxygen-terminated $RuO_2(110)$ (a) and the bridging oxygen-terminated $RuO_2(100)$ (b) surfaces. Large balls represent oxygen, and small balls represent ruthenium atoms of $RuO_2(100)$. The coordinatively unsaturated Ru atom (cus) as well as the bridge bonded and 3-fold coordinated lattice O atoms are indicated by arrows. The bridge bonded O atoms are directly coordinated to the cus-Ru atoms on $RuO_2(100)$, while these are well-separated on $RuO_2(110)$. The surface energies (determined by DFT calculations) are indicated.

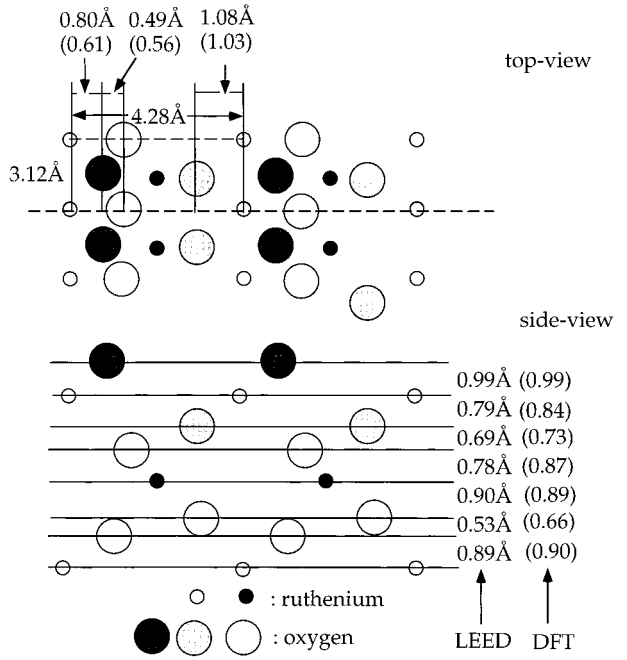


**Figure 8.** Top view and side view of the optimum surface geometry of the $RuO_2(100)$ as determined by LEED and DFT calculations (values are given in parentheses). All values are in angstroms. The corresponding layer spacings in bulk $RuO_2$ are 0.45 and 0.90 Å.

calculation). This binding energy is markedly lower than on $RuO_2(110)$ where CO molecules are bound by 1.2 eV. In Figure 10 we present corresponding CO and $CO_2$ TD spectra of $RuO_2$-(100) after having exposed the surface to 10 langmuirs of CO at 200 K. CO desorption takes place between 200 and 500 K.

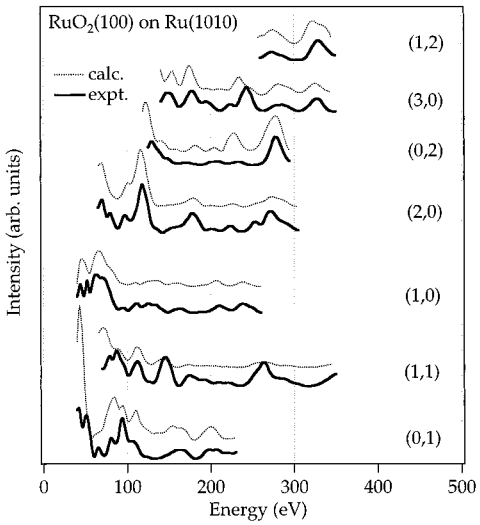


**Figure 9.** Comparison of experimental and calculated LEED *I*/*E* data for the best-fit model of the $RuO_2$(100) surface (cf. Figure 8). The overall $R_P$-factor is 0.31.

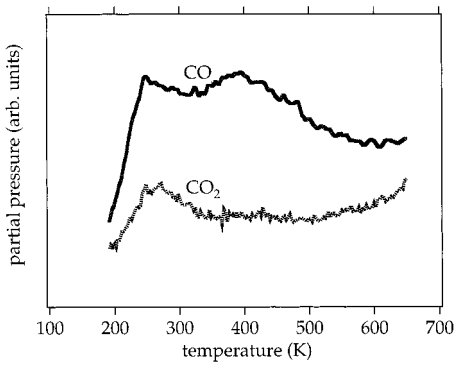


**Figure 10.** CO and $CO_2$ TD spectra taken after the $RuO_2$(100) surface was exposed to 10 langmuirs of CO at 200 K.

The relatively high CO desorption temperature is already indicative of cus-Ru atoms present on the $RuO_2$(100) surface. DFT investigations on $RuO_2$(110) have shown that only the cus-Ru atoms can bind CO molecules so strongly (via the so-called Blyholder model).[22] Concomitant with CO, also $CO_2$ is produced and leaves the $RuO_2$(100) surface with a maximum flux at a sample temperature of 280 K. A reasonable reaction pathway is that the adsorbed CO molecule catches the bridging O atom which is coordinated to the same cus-Ru atom as CO. This kind of oxidation reaction, in which lattice oxygen from the oxide is consumed, goes back to Mars and van Krevelen[23] and has been verified on atomic scale on $RuO_2$(110).[4] After recombination of CO and $O_{br}$ the cus-Ru atoms are only 3-fold coordinated on $RuO_2$(100) which may be too low so that the Ru atoms agglomerate in small Ru clusters.

The electronic structure of $RuO_2$(100) was examined by the pseudo-valence charge density difference maps, which are defined as the difference between the total valence electron density (as determined by DFT calculations) and a linear superposition of radially symmetric atomic charge density.[24] These plots reflect the hybridization of Ru and O upon bond formation in the solid phase. The most prominent feature in this Figure 11 is the substantial charge transfer along the Ru−O bonds and the charge accumulation along the Ru−Ru bonds. The $RuO_2$(110) and the $RuO_2$(100) surfaces are electronically quite similar, as demonstrated in Figure 11. The cus-Ru atom on the (100) surface reveals—similar to the (110) surface—a dangling bond (dashed contour lines protruding into the vacuum

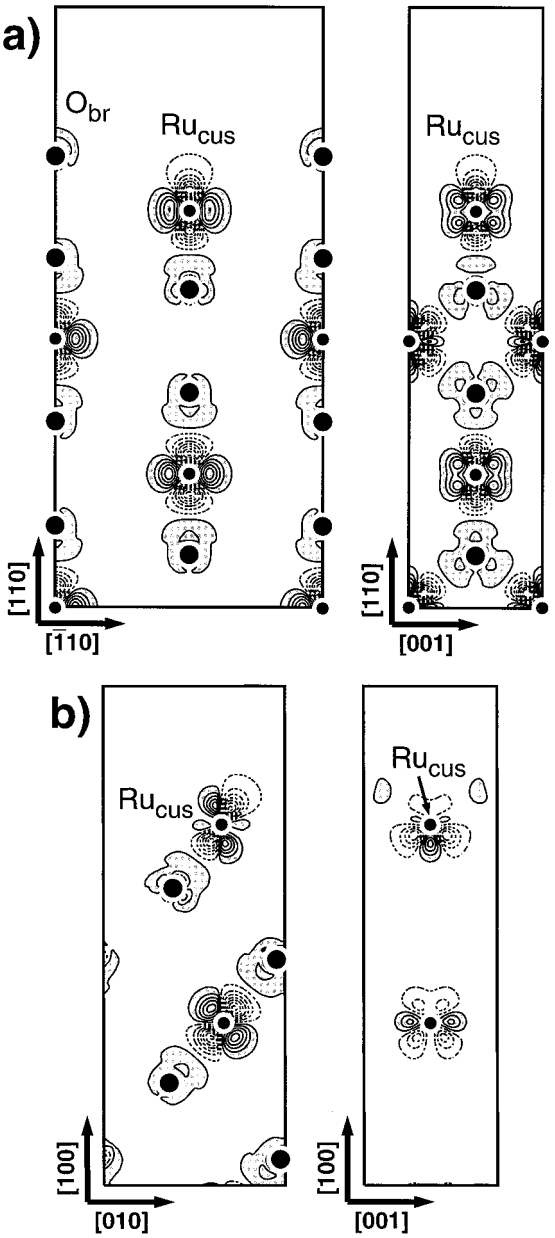


**Figure 11.** Pseudo-valence charge density contour plots of the (a) $RuO_2$(110) surface in comparison with the (b) $RuO_2$(100) surface cut through the cus-Ru atoms. These plots are defined as the difference between the total valence electron density and a linear superposition of radially symmetric atomic charge densities. Contours of constant charge density are separated by 0.15 eV/Å$^3$. Electron depletion and accumulation are marked by dashed and solid lines, respectively. In addition, regions of electron accumulation are shadowed.

region) which might explain naturally the activity of the cus-Ru atoms toward chemisorption of other molecules. Different from the cus-Ru atom on $RuO_2$(110), the cus-Ru atom on $RuO_2$-(100) is also directly coordinated to the undercoordinated bridging O atom. This is reflected by a change in the hybridization of the surface cus-Ru atom on $RuO_2$(100) (cf. Figure 11b) if compared to the hybridization of a bulk Ru atom. Quite in contrast, the hybridization of surface cus-Ru atoms on $RuO_2$-(110) is preserved (cf. Figure 11a).

The different hybridization of cus-Ru atoms and the direct contact of cus-Ru and bridging O atoms on $RuO_2$(100) should have serious impact on the activity and selectivity of such active centers for the partial oxidation of hydrocarbons. With CO adsorption this difference is already evident. Obviously, the

direct attachment of undercoordinated O and Ru atoms at the $RuO_2(100)$ surface allows only for a moderately strong CO bonding (0.7 eV) in comparison to $RuO_2(110)$ (1.2 eV).

## 4. Summary

We determined the surface structure of $RuO_2(100)$ grown on $Ru(10\bar{1}0)$ by employing the techniques of quantitative LEED and DFT calculations. The $RuO_2(100)$ film grows lattice-matched with its [010] direction along the [0001] direction of $Ru(10\bar{1}0)$, while it grows incommensurately along the $[\bar{1}2\bar{1}0]$ direction. The lattice constant of $RuO_2(100)$ is 4.5% compressed along the [010] direction and fully relaxed in the [001] direction. The $RuO_2(100)$ surface is terminated by bridging O atoms, which are directly coordinated to the cus-Ru atoms, revealing a bond length of 2.01 Å. The other Ru−O bond lengths are in the range of 1.90−2.05 Å, typical for bulk $RuO_2$. Structural deviations from the bulk-truncated $RuO_2(100)$ surface are mainly caused by the unidirectional compression of the epitaxial $RuO_2$-(100) film on $Ru(10\bar{1}0)$. CO molecules are bound by 0.7 eV on $RuO_2(100)$ consistent with a desorption state above 250 K. In comparison with the $RuO_2(110)$, the adsorption of CO on $RuO_2$-(100) should proceed in terminal position over the cus-Ru atoms consistent with our DFT calculations.

**Acknowledgment.** We thank K. Jacobi for lending us the $Ru(10\bar{1}0)$ sample and Marcus Knapp for valuable discussions. We acknowledge T3E computing from the ZIB.

## References and Notes

(1) Peden, C. H. F.; Goodman, D. W. *J. Phys. Chem.* **1986**, *90*, 1360.

(2) (a) Böttcher, A.; Niehus, H.; Schwegmann, S.; Over, H.; Ertl, G. *J. Phys. Chem.* **1997**, *101*, 11185. (b) Böttcher, A.; Rogozia, M.; Niehus, H.; Over, H.; Ertl, G. *J. Phys. Chem.* **1999**, *103*, 6267.

(3) Kim, Y. D.; Over, H.; Krabbes, G.; Ertl, G. *Topics in Catal.* **2001**, *14*, 95.

(4) Over, H.; Kim, Y. D.; Seitsonen, A. P.; Wendt, S.; Lundgren, E.; Schmid, M.; Varga, P.; Morgante, A.; Ertl, G. *Science* **2000**, *287*, 1474.

(5) Kim, Y. D.; Seitsonen, A. P.; Over, H. *Surf. Sci.* **2000**, *465*, 1.

(6) Over, H.; Lundgren, E.; Schmid, M.; Varga, P. Unpublished material.

(7) Lin, W. F.; Zei, M. S.; Kim, Y. D.; Over, H.; Ertl, G. *J. Phys. Chem.* **2000**, *104*, 6040.

(8) Over, H.; Bludau, H.; Skottke-Klein, M.; Moritz, W.; Ertl, G. *Phys. Rev. B* **1992**, *46*, 4360.

(9) Moritz, W. *J. Phys. C* **1983**, *17*, 353.

(10) (a) Kleinle, G.; Moritz, W.; Ertl, G. *Surf. Sci.* **1990**, *226*, 119. (b) Over, H.; Ketterl, U.; Moritz, W.; Ertl, G. *Phys. Rev. B* **1992**, *46*, 15438. (c) Gierer, M.; Over, H.; Moritz, W. Unpublished material.

(11) Pendry, J. B. *J. Phys. C* **1980**, *13*, 937.

(12) Perdew, J. P.; Burke, K.; Enzerhof, M. *Phys. Rev. Lett.* **1996**, *77*, 3365.

(13) Troullier, N.; Martins, J. L. *Phys. Rev B* **1993**, *43*, 1991.

(14) Schwegmann, S.; Seitsonen, A. P.; De Renzi, V.; Dietrich, H.; Bludau, H.; Gierer, M.; Over, H.; Jacobi, K.; Scheffler, M.; Ertl, G. *Phys. Rev. B* **1998**, *57*, 15487.

(15) Stampfl, C.; Schwegmann, S.; Over, H.; Scheffler, M.; Ertl, G. *Phys. Rev. Lett.* **1996**, *77*, 3371.

(16) Kim, Y. D.; Wendt, S.; Schwegmann, S.; Over, H.; Ertl, G. *Surf. Sci.* **1998**, *418*, 267.

(17) Klein, R.; Siegel, R.; Erickson, N. *J. Vac. Sci. Technol.* **1979**, *16*, 489.

(18) Poulsston, S.; Tikhov, M.; Lambert, R. M. *Surf. Rev. Lett.* **1994**, *1*, 655.

(19) Orent, T. W.; Hansen, R. S. *Surf. Sci.* **1977**, *67*, 325.

(20) Hazen, R. M.; Finger, L. W. *J. Phys. Chem. Solids* **1981**, *42*, 143.

(21) Glassford, M. K.; Chelikowsky, J. R. *Phys. Rev. B* **1993**, *47*, 1732.

(22) Kim, Y. D.; Seitsonem, A. P.; Over, H. *Phys. Rev. B* (in press).

(23) Mars, P.; van Krevelen, D. W. *Chem. Eng. Sci.* **1954**, *3* (Suppl.), 41.

(24) Hirschfeld, F. L. *Isr. J. Chem.* **1977**, *16*, 226.